Eddy Current Imager for the Detection of Buried Flaws in Large Metallic Structures

Pierre-Yves JOUBERT, Yohan LE DIRAISON, Jean PINASSAUD, Laboratoire SATIE, Ecole Normale Supérieure de Cachan, Cachan Cedex, France.

Abstract. The authors present a prototype of an eddy current imager dedicated to the high speed inspection of aeronautic riveted lap joints. The system provides high resolution images of the complex magnetic field distribution at the surface of the inspected structure, and allows thorough defect characterization to be achieved. The system was implemented for the detection of buried notches placed next to the rivets of a laboratory made lap joint mock-up. Associated to a dedicated signal processing method, the system allows 6 mm deep EDM notches (0.2mm×3mm×7mm) to be detected and localized within the depth of the inspected structure, and appears very promising for the characterization of buried defects in actual riveted lap joints.

1. Introduction

The detection of corroded areas and fatigue cracks is a major preoccupation for the maintenance of ageing aircraft. Indeed aeronautic structures, such as wing or fuselage riveted lap joints, are submitted to strong mechanical and climatic constraints. These constraints may induce the apparition of cracks, specially in the vicinity of the rivets. Cracks can then propagate from one rivet to the others, specially in the areas already weakened by corrosion, and lead to dramatic issues. In order to prevent accidents as to optimize the lifetime of the structures, it is necessary to detect the defects in their early stage with the best possible accuracy and reliability.

Among the available non-destructive evaluation techniques, eddy currents (EC) sensors are widely used for the inspection of aluminium based alloy riveted structures, since they are sensitive to defects and easy to implement. However a typical commercial aircraft is constituted of tens of thousands of rivets ; the use of conventional EC sensors featured by a reduced number of sensing elements implies time consuming - and therefore expensive - inspection procedures. In this context, efforts have been made to develop alternative solutions such as the magneto optic / eddy current imager (MOI) designed by Physical Research Instrumentation (PRI) in the early 90's, dedicated to the real time visualization of images relative to the presence of cracks and corrosion in a large inspection area (76mm diameter) [1]. The MOI combines the use of an inductor required to induce eddy currents into the inspected structure, and the use of the Faraday rotation occurring in a magneto-optic (MO) sensor operating in polarized light, to locate high values of the normal component of the resultant magnetic field at the surface of the structure.

The designer evaluates that the inspection time should be reduced by a factor 1/10 in comparison with conventional EC sensors [1]. However, due to the use of a MO indicator featured by a "two-state" magnetization loop, the MOI provides only "two-level" images [1-2]. These two levels are resulting from a binary comparison to an adjustable polarization

magnetic field threshold. Therefore, the operator is compelled to systematically adjust the threshold level during inspections, in order to retrieve the most relevant image relatively to the considered defect. This adjustment is rather empirical and requires multiple inspection of the same area with different threshold values in order to guaranty a reliable detection rate. Two major drawbacks derive from this "two-level" detection. Firstly the necessity of multiple scanning is time consuming and actually limits the inspection efficiency. Secondly, the obtained binary images allow poor defect characterizations to be achieved, even with the help of experimented operators or dedicated signal processing [3]. Finally, serpentine structures [2] due to the minority magnetic domains of the MO garnet, cloud the resulting images and actually limit the defect detection possibilities, specially in the case of subsurface defects.

To overcome these drawbacks, the SATIE laboratory, in collaboration with the ONERA[1] and the LMB[2], has studied the principle of a linear MO/EC imager, able to provide a complex EC image linearly related to the 2D distribution of the normal magnetic field component, at the surface of the inspected structure. The method was patented in 2003 [4], and showed significant improvements, firstly because no threshold adjustment is required and secondly because high signal-to-noise-ratio true EC images were obtained. Furthermore, the high quality of the images will allow advanced signal processing algorithms, such as image inversion, to be implemented in the future for a thorough defect characterisation.

In this paper, the authors present an EC imager prototype dedicated to the detection of buried defects in riveted lap joints. After a short presentation of the measurement principle, the EC imager prototype will be described and implemented for the inspection of a laboratory made lap joint mock-up featuring buried calibrated notches. Finally a signal processing method developed to enhance the detection and characterization of the buried defects will be presented and discussed.

2. Eddy Current Imager

2.1. Basic Principle

The principle of the linear EC imager was described in [5] and is presented in Figure 1. A specific eddy current inductor is used to excite the inspected material, and is fed by a sine wave of adjustable frequency. The presence of a defect in the structure induces variations of the normal component of the magnetic field distribution at the surface of the material, $H_z(x,y)$, which are sensed by a linear MO sensor by Faraday effect. The sensor is integrated in the optical set-up so that the variations of the magnetic field are linearly translated into variations of intensity of a light beam measured by a CCD camera. The acquisition rate of the used camera (25 images/s) being far smaller than the frequency of the electromagnetic field (up to 20 kHz), the images are obtained thanks to a stroboscopic approach, followed by a digital image lock-in [5-6] used to obtain the real and imaginary parts of the magnetic field.

[1] Office National d'Etudes et de Recherche Aérospatiales
[2] Laboratoire de Magnétisme de Bretagne

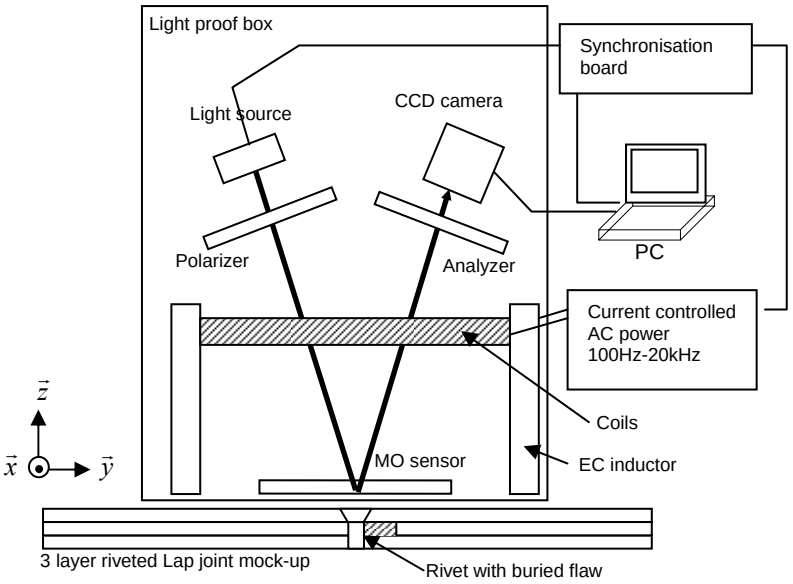

Figure 1. Schematic presentation of the eddy current imager

2.2. Magnetic Field Sensing

A light source associated with an adequate polarizer generates a linearly polarized light beam which flows through the linear MO sensor. If the sensor is excited by a normal magnetic field $\vec{H}_z$ so that :

$$H_z(t) = H_{0z}\sin(2\pi ft + \Psi) \tag{1}$$

where Ψ is the phase shift of the field by reference to the excitation current, the polarization angle is rotated by an angle ρ linearly related to the magnetic field for an adequate MO sensor, as expressed by :

$$\rho(t) = K.H_z(t) \tag{2}$$

where K is a constant depending on the nature of the MO sensor and the light wavelength. The luminous flux Φ_{det} received by the photodetector at the output of the analyzer, is then expressed by :

$$\Phi_{\det}(t) = e_0^2\cos^2[\nu + \rho(t)] \tag{3}$$

where e_0 designates the intensity of the light beam, and ν is the angle between the polarizer and the analyzer. A first order development of the expression of Φ_{det} gives [5]:

$$\Phi_{\det}(t) \approx e_0^2[\Phi_0 - \Phi_1\sin(2\pi ft + \Psi)] \tag{4}$$

where Φ_0 and Φ_1 are the mean value and the amplitude of the first harmonic of Φ_{det}, respectively, and are expressed by :

$$\begin{cases}\Phi_0 = \frac{1}{2}[1+\cos(2\nu)] \\ \Phi_1 = k_F\,H_{0z}\sin(2\nu)\end{cases} \tag{5}$$

Finally, to get rid of the residual non-uniformity of the pixel lightening, one can consider the ratio :

$$\frac{\Phi_1}{\Phi_0} = k_F\frac{2\sin(2\nu)}{1+\cos(2\nu)}\times H_{0z} \tag{6}$$

which is proportional to the intensity of the wanted magnetic field. In practice, a reflective layer is deposited on the bottom face of the garnet, so that the light beam is reflected after flowing through the sensor. In this way, the Faraday effect is doubled since the light beam crosses the MO sensor twice. Finally, Φ_0 and Φ_1 are measured thanks to a stroboscopic approach using a synchronized CCD camera. The light source is modulated and synchronized with the excitation frequency, in order to sample the magnetic field H_{0z}. At a given instant within the period of the excitation current, the CCD camera makes N_a image acquisitions, N_a being chosen large enough for noise reduction purposes. The operation is repeated at N_p different instants chosen within the period of the excitation current. From this set of images, it is then possible to compute the amplitude and the phase of the magnetic field according to equation (6).

2.3. Eddy Current Imager Prototype

The EC imager prototype was integrated in a lightproof box including the optical set-up, the eddy current inductor, the linear MO garnet and the CCD camera (Figure 1). The optical set-up is constituted of two polarizers, a LED array associated with a lens set and designed to produce a uniform and linearly polarized light beam.

The EC inductor is composed of a two pole magnetic circuit excited by two bobbin coils winded and connected so that the induced magnetic flux uniformly flows from one magnetic pole to the other through the inspected material along the *y* axis (see Figure 1) and the eddy current uniformly flows in the inspection area along the *x* axis. The geometry of the EC inductor was studied thanks to 3D finite element computations, in order to optimize both the uniformity of the normal magnetic field distribution in the inspection area, and the intensity of the induced eddy currents for a given excitation current [7].

The MO garnet is a constituted of a 6µm layer made of a $(GdPrBiTm)_3(AlFe)_5O_{12}$ iron oxide, realized by liquid-phase epitaxial growth on a 76 mm diameter SGGG substrate. The garnet features magnetic domains oriented perpendicularly to the plane of the garnet so that the sensor is sensitive to the normal magnetic field. The domain periodicity is around 15 µm which is far less than the required spatial resolution necessary to correctly sample the field distribution [5]. Placed in the (*x*, *y*) plane (Figure 1), the garnet induces a Faraday rotation ρ of the light beam polarization [5] according to:

$$\rho = k_F \vec{M} \vec{k} \tag{7}$$

where k_F is a constant depending on the composition and geometry of the garnet and of the light wavelength, $\vec{M}$ is the magnetization and $\vec{k}$ the direction of the light beam (which is, in practice, almost parallel to the *z* axis). The magnetization loop of the MO sensor is hysteresis free and linear in the range -8000 to +8000 A/m, therefore one can consider that the obtained Faraday rotation is proportional to the amplitude of $\vec{H}_z$ at the surface of the inspected structure.

A digital control board was developed to synchronize the AC current source and the LED array in order to carry out the stroboscopic approach. Both the camera and the digital board are controlled by a PC by the use of a dedicated software application which also computes the real and imaginary parts of the magnetic field, from the $N_a \times N_p$ images acquired by the camera. The image acquisition was actually carried out with a 12-bits 1.3Mpixel CCD

camera, and the optical setup was adjusted so that 45 mm diameter EC images are provided with a spatial resolution of 100µm along both the *x* and *y* axis (Figure 1).

3. Experimental results

3.1. Riveted Lap Joint Mock-up

The EC imager prototype was implemented for the inspection of a laboratory made riveted lap joint. The mock-up is constituted of three identical 3 mm thick plates made of an aluminum based alloy, featured by a 20MS/m electrical conductivity and a unity relative magnetic permeability. The plates are fastened by 6 mm diameter head aluminum rivets. EDM notches were realized next to some of the rivets, to simulate fatigue cracks growing from the rivets. The notches are placed in the second plate (3mm deep, left hand side of rivets n°3 and n°4) or the third plate (6mm deep, left hand side of rivets n°8 and n°9), as depicted in Figure 2. The notches are 200 µm wide, 3 mm deep and 7 to 12 mm long.

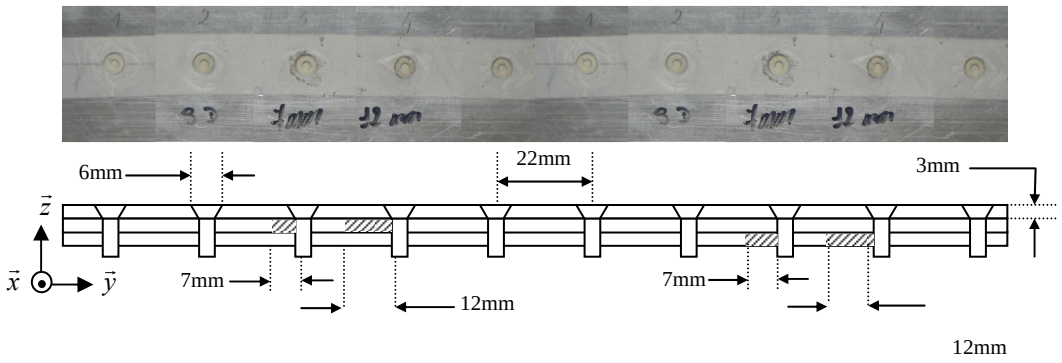

Figure 2. Laboratory made lap joint mock-up with sound and flawed rivets. Reconstituted photograph (top view), and schematic representation (side view).

3.2. Experimental Conditions and Results

The EC imager was implemented with a 5A excitation current flowing in the inductor, at the frequencies of 200Hz and 700Hz which provide skin depths of 8 mm and 4.3 mm, respectively. The images were obtained with acquisition parameters of N_a = 10 and N_p = 10 and an acquisition time of 15 seconds. The real and imaginary parts of the resulting EC images are computed by reference to the excitation current flowing in the EC inductor, which was used to define the phase shift reference. In this study, 10 elementary EC images were realized around the 10 rivets. The images were reshaped and gathered in one resulting EC image by concatenation, after background removal (suppression of the residual mean value of the images, determined in unflawed areas).

The resulting EC images are presented in Figure 3, in real and imaginary parts. Since the EC flow along the *x* axis, the EC signatures of the rivets are constituted of two anti-symmetrical patterns, for both real and imaginary parts, appearing on each side of the rivets along the *y* axis. These patterns are relative to the distribution of the normal component H_z induced by the modification of the EC flowing in the vicinity the rivets. These patterns are modified in shape, amplitude and phase in the case of a flawed rivet. Here, the presence of the buried notches are observable around rivets n°3, 4, 8 and 9 on the EC image obtained at

200Hz (images A and B), and only around rivets n°3 and 4 on the EC image obtained at the frequency of 700Hz (images C and D), since the skin depth is insufficient for the visualization of the deeper notches.

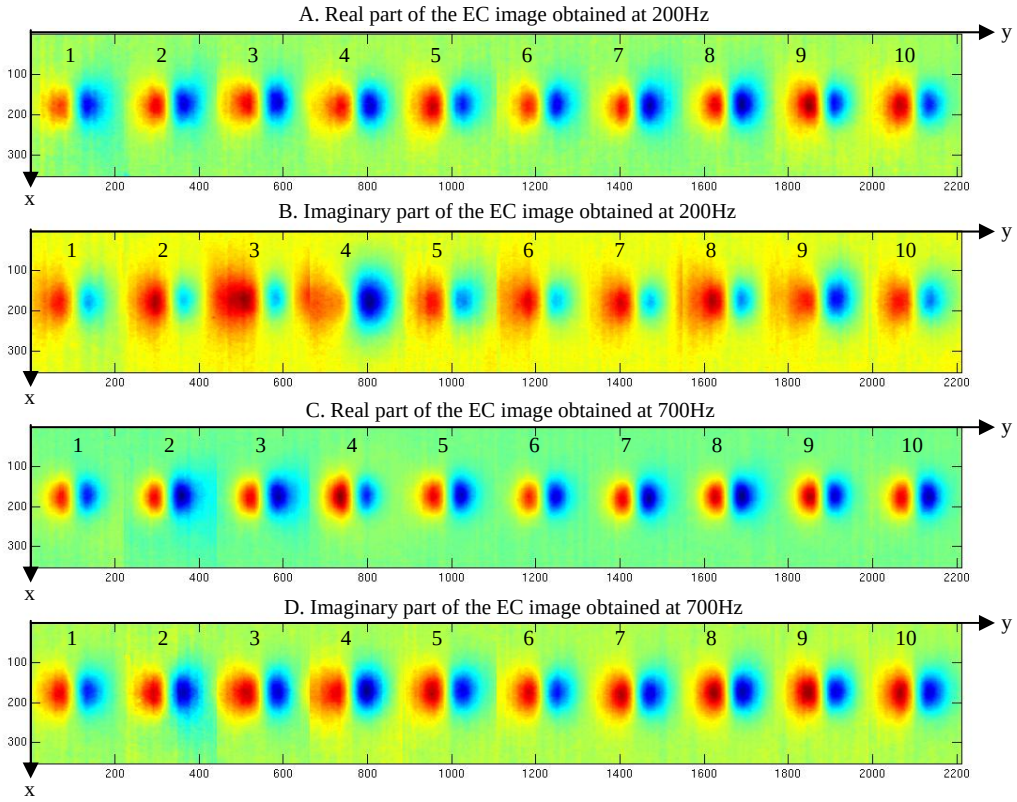

Figure 3. EC images obtained by the inspection of the riveted lap joint laboratory mock-up. Colours are arbitrary and the sampling step is 100µm along the x and y axes.

4. Signal processing for the detection of buried flaws.

In this section a signal processing method is proposed in order to enhance the detection and characterization of the buried flaws. Indeed the EC signatures due to the defects are rather difficult to analyze from the raw EC images, firstly because they are masked by the presence of the rivets, and secondly because of the attenuation of the EC intensity with the penetration depth in the material. The objective of the method is to find a more adequate representation space in which the signatures of the rivets and of the defects can be separately visualized. For that purpose, a source separation method based on a principal component analysis (PCA) is a good candidate [8].

4.1. Basic Principle of the Signal Processing Method

Assuming that the EC imager can be modelled by :

$$M = T.\,S \tag{8}$$

where M is the measurement matrix, T is the transfer matrix of the EC imager, and S are the physical sources, including the signatures of the rivets and of the flaws. In the ideal case, a source separation would consist in the estimation of the sources from the measurement M as expressed by:

$$S = T^{-1}.\ M. \tag{9}$$

In practice, the coefficients of the transfer matrix are unknown. However, a PCA allows the different sources to be separated. Indeed, the PCA of a measurement matrix M consists in the projection of M on the subspace defined by the eigenvectors associated to the eigenvalues of the covariant matrix MM^t [8]. The resulting matrix R^{PCA} is then expressed by:

$$R^{PCA} = (Q^{PCA})^t \cdot M \tag{10}$$

where Q^{PCA} is the matrix of the eigenvectors of MM^t and Δ^{PCA} is the matrix of the associated eigenvalues arranged by descending order, so that:

$$MM^t = Q^{PCA}\Delta^{PCA}(Q^{PCA})^t\,. \tag{11}$$

Under the hypothesis that the sources are uncorrelated and that the row vector of T are orthogonal, then it can be demonstrated [8] that the PCA realizes a source estimation, expressed by:

$$\hat{S} = (Q^{PCA})^t \cdot M \tag{12}$$

in which the separated sources of M are the rows of $\hat{S}$, arranged by decreasing order with respect to their variance [8]. One must note that the implementation of the signal processing method requires the acceptance of the hypothesis expressed above, which are not *a priori* obvious to assume. However, if these hypothesis are not entirely fulfilled, it is known that the PCA allows a source *rejection* - rather than an actual *separation* - to be achieved [8]. The rejection is sufficient here as it is *a posteriori* verified by the obtained results presented in section 4.2.

4.2. Implementation and Results

In this study, the objective is to separate three sources: the signatures of the rivets, the signatures of the buried flaws in the second plate, and the signatures of the buried flaws in the third plate, which all contribute, in decreasing order, to the provided images. To that purpose, the real and imaginary parts of the EC images obtained at 200Hz and 700Hz (presented in Figure 3) are chosen to constitute four different measurement data used to build the measurement matrix M. The frequencies were chosen so that the data contain various information relative to the inspected structure, thanks to the variation of the skin depth. As a result, four separated sources are expected to appear in the following order:

- rivets,
- flaws in the second plate,
- flaws in the third plate,
- 4th source (unidentified).

The method was implemented at each line of the EC images using equation (12), and resulting images were build by concatenation of the results obtained at each lines. The resulting images are presented in Figure 4, after integration along the y axis, for image enhancement purposes. As expected, the presence of the rivets appear as the first source (image E), since the signatures of the rivets show the higher variance. The 2nd source is relative to the buried flaws in the second plate (image F), and the 3rd source to the buried

flaws in the 3rd plate, because of the attenuation of the signature amplitude with the depth of the defect. The last source (image H) is here unidentified and irrelevant for the characterization of the structure (and could be attributed to residual noise, tilt angle in the rivet position, ...). It can be observed that the buried flaws are clearly detected and localized in the (x,y) plane (images F and G) thanks to an efficient rejection of the rivet signature, although the spatial resolution decreases with the depth of investigation (image G). Furthermore, the proposed method allow the buried defects to be correctly localized within the depth of the structure, which proves to be very promising for classification applications.

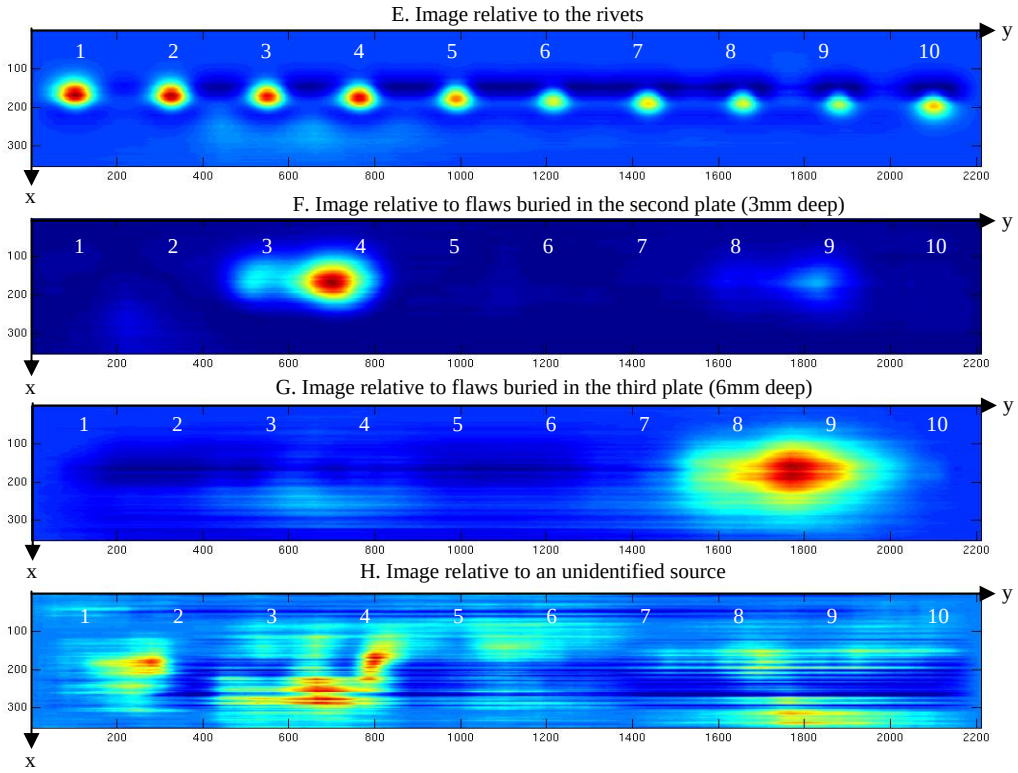

Figure 4. Images obtained after signal processing for the detection of the buried flaws. Colours are arbitrary and the sampling step is 100µm along the x and y axes.

5. Conclusion

In this paper, the authors present a prototype of an eddy current imager dedicated to the high speed inspection of aeronautic riveted lap joints. The system provides a true measurement of the complex magnetic field at the surface of the inspected structure and allows thorough defect characterization to be achieved. The prototype was implemented for the detection of buried defects in a laboratory-made riveted lap joint. A proposed signal processing method based on a principal component analysis allowed 3mm and 6mm deep buried notches placed next to the rivets to be correctly detected and localized, and reveals great potential for classifications purposes. Further works will focus on the evaluation of the device on real lap joints - featuring actual fatigue cracks and corrosion - and on the extension of the signal processing method to a defect classification scheme.

References

[1] G.L. Fitzpatrick et al., “Magneto-optic / eddy current imaging of ageing aircrafts”, Material Evaluation, pp. 1402-1407, (1993).
[2] Development of an improved magneto optic/eddy current imager, final report DOT/FAA/AR-97/37, Office of Aviation Research, Washington DC, 20591, 1998.
[3] J.M. Decitre, M. Lemistre, F. Lepoutre, “Defect localization in metallic structures by magneto-optic image processing”. Review of Progress in Quantitative Non Destructive Evaluation Vol.19, AIP Conference Proceedings 509, Montréal, Canada, 25-30 juillet 1999, pp 889-896.
[4] Linear Magneto optic imaging device for the non destructive evaluation of aluminium aeronautic structures. Patent n° FR0307850, 2003.
[5] P.-Y. Joubert and J. Pinassaud, Linear magneto-optic imager for non-destructive evaluation , Sensors and Actuators A: Physical, Volume 129, Issues 1-2, 24 May 2006, Pages 126-130
[6] S. Grauby, “High frequency photoreflectance photothermic imaging using a natural light CCD camera associated with a multiplexed lock-in”, Ph.D. Thesis, University of Paris VI, 2000.[in French]
[7] Y. Le Diraison, P.-Y. Joubert, J. Pinassaud, « 3D Finite Element modeling of an EC imager », 7th International Symposium on Electric and Magnetic Fields - Aussois, France, June 19-22, 2006.
[8] G. Saporta, *Théories et méthodes de la statistique*, Institut Français du Pétrole, Technip. br. in 8. 386 p, 1978. [in French]

Acknowledgmenents

The authors thank Pr. C. Dolabdjian for useful discussions and for the loan of lap joint mock-ups.